# Experimental investigation of mesoscale variability of clear spruce mechanical properties in the radial direction

**Alireza Farajzadeh Moshtaghin[1], Steffen Franke[2], Thomas Keller[1], Anastasios P. Vassilopoulos[1*]**

[1] Composite Construction Laboratory (CCLab), Ecole Polytechnique Fédérale de Lausanne (EPFL), Station 16, Bâtiment BP, CH-1015 Lausanne, Switzerland

[2] Institute for Timber Construction, Structures and Architecture, Bern University of Applied Sciences, Solothurnstrasse 102, CH-2500 Biel 6, Switzerland

ABSTRACT

The aim of this work is the investigation of mesoscale/local variability in mechanical properties of clear timber in the radial direction. Clear Norway spruce wood, Picea abies, was used for cutting specimens of different lengths with a small cross-sectional area of 4×4 $mm^2$, in the radial direction of timber boards, and tested under tensile loading. In some boards, specimens were positioned regularly and, in some others, randomly, and local deformations in each specimen were measured during the tests. The results indicate a significant variability in the specimens' elastic moduli and strengths. A correlation between the mesostructure of clear timber and mesoscale/local variability of the transverse elastic modulus in the specimens was observed. Specimens' failures were classified and a reasonable correlation with the corresponding strength values was observed.

**Keywords*:*** Clear spruce, transverse mechanical properties, variability, mesoscale, length effect

## 1. Introduction

Wood is a natural highly anisotropic fiber composite with mechanical properties showing considerable scatter [1-3]. Different factors e.g. age, location of timber within the tree, structural imperfections, genetics, tree social status and load history, can affect the material properties of timber taken from the same species, and grown in the same geographical location

* Corresponding Author: e-mail: anastasios.vassilopoulos@epfl.ch Tel.: +41 21 69 36 393

and under the same local growth conditions. Other factors such as decay and post-treatments like incising, impregnation and modification can also be mentioned.

The effect of the high scatter of timber elastic properties on the response of timber structures has received less attention in the literature than the effect of the scatter of strength [4, 5]. In the few works that take the statistical variability of the elastic modulus into account, when assessing the structural response, the local point-by-point variability, i.e. the spatial variability, is commonly neglected [6, 7]. In the context of materials characterization, the term "mesoscale" refers to measurements performed on a local scale with a length range of a few millimeters, as shown in Fig. 1. Therefore, local variability is equivalent to "within-specimen" variability. As such, timber boards and tree dimensions are at the macroscale. This local variability of the elastic modulus can affect the local stress state of the material, which can be critical in estimating the failure probability under external loading [8].

The mean strength of timber decreases as its volume increases due to the size effect on the strength. A small number of works have used pure tensile tests, on specimens of different sizes, to investigate the size effect on the strength of clear timber. In [9], a length effect parameter was introduced by Zhu et al. to quantify the size effect, due to the length change, on the longitudinal tensile strength of Japanese larch wood. Dill-Langer et al. [10] conducted longitudinal tensile experiments on two groups of specimens composed of spruce wood and observed that the volume of the material significantly affects the strength. In a recent study [11], a new method for investigating the size effect on the bending behavior of small-sized specimens cut from wood and veneer has been developed based on the three-point bending test. According to the results, the size effect on the bending strength and the bending modulus are significant. A few experimental works have been devoted to the effect of size on the transverse strength of clear timber [1, 12-15], mainly focusing on glued-laminated materials.

The longitudinal mechanical properties of timber have been intensively investigated, while fewer efforts were devoted to the investigation of the timber transverse properties, see e.g. [4]. This is primarily because of the common applications of timber as beams and truss elements where longitudinal stresses are dominant. In other applications however, such as mechanical and adhesively-bonded timber joints, the transverse mechanical properties are of critical importance. Nevertheless, due to the anisotropic nature of timber, those properties are significantly lower than the longitudinal ones [16-18]. On top of this, transverse mechanical properties are different in the radial and in the tangential direction. Because of the natural local variability of timber, and the waviness of the growth rings of each tree, the local properties

measured in the transverse direction of boards, cut in the radial plane of the tree, as shown in Fig. 1, can deviate from the local radial direction of annual rings, which is perpendicular to the annual ring at any point. The deviation depends on the growth ring angle at any point of interest.

Previous transverse tensile experiments were mostly carried out on bulk cubic or glulam specimens in order to comply with the EN standard [19], which recommends a glued laminated timber composed of solid timber blocks as the testing specimen. The results of such experiments show a lower level of variability in transverse strength compared to that exhibited by clear timber experiments due to the homogenization that can be achieved in laminated wood specimens. The size effect on the transverse strength of small clear specimens has not been investigated previously at the mesoscale.

Experimental results from small specimens for the investigation of the size effects at the mesoscale of clear timber are missing in the literature, although they are required to accurately simulate local failures in clear wood used in wooden structural components.

This paper addresses the literature need for data on the mesoscale variability of transverse mechanical properties of clear Norway spruce wood (*Picea abies*). Norway spruce wood was selected, since it is commonly used in constructing timber structures due to high mechanical properties per unit weight and relatively high grow rate [20]. Three groups of specimens of different lengths were cut in regular and random ways from boards of 4mm thickness and their quasi-static behavior was experimentally investigated under tensile loading in the transverse direction. In addition to the global displacement monitoring, the local deformations along the length of each specimen were measured, and the effect of the mesostructure of the clear timber on the local elastic modulus was examined.

## 2. Experimental program

### *2.1. Material and conditioning*

Norway spruce wood was used for the specimens' preparation in this study. Sapwood and juvenile wood were avoided. All specimens were conditioned to 12% moisture content according to the ASTM standard D143-14 [21] and tested at the laboratory temperature of 22 ± 3 °C. The average density of the specimens after conditioning was 441.2 ± 14.4 kg/m$^3$.

### *2.2. Spruce boards*

Ten boards of 4 mm thickness were cut from the same batch of spruce lumbers in the radial-longitudinal plane. All specimens were cut from the same batch of lumbers ordered from one timber factory. It can be assumed that all lumbers were from the same tree, or from different trees, with a similar age grown at the same area. No investigation regarding the position of specimens relative to the pith was conducted in this paper. The approximate location of the boards within the tree is shown schematically in Fig. 1. Since the tree trunk is not a perfect cylinder the actual boards approximately cross the pith. This can be confirmed by the geometry of the growth ring patterns (see Figs. 2-5). The measured local mechanical properties in the transverse direction of the boards do not always correspond exactly to the local radial direction of annual rings, which can vary point-by-point, therefore the measured values can be considered as effective radial properties. This depends on the deviation angle, a term used in this work to denote the angle between latewood strip (local tangential direction) and the perpendicular to the specimen axis. In seven boards, specimens of specific lengths were positioned regularly, referred to as regular boards (REB1-REB7). The other three boards were used for cutting randomly positioned specimens of different lengths and are designated as random boards (RAB1-RAB3). Each timber board can generally have a different level of average transverse strength, due to the fact that it is cut from a different position within the tree trunk. Therefore, when specimens of different lengths are cut from the same boards, as in the RABs, the comparison of strengths of specimens of different lengths can be more meaningful, since such a comparison then excludes the variability between boards.

Specimens of different lengths were fabricated by using a CNC machine. A cross-sectional area of 4×4 $mm^2$ was considered for all investigated specimens. Representative specimens are shown in Fig. 2a, while specimen geometry is shown in Fig. 2b. The lengths, L1, of the middle zone (nominal length) are 8, 32 and 120 mm. L2 is 20 mm, for specimens of 8 mm and 32 mm lengths, and 9 mm, for specimens of 120 mm length. A typical specimen of 32-mm length mounted in the testing rig is shown in Fig. 3. After conducting a number of preliminary experiments, 226 specimens were tested during the main program and the experimental results are reported in this work.

Figure 4a-c shows the REBs used for cutting specimens of different lengths. Two boards for specimens of 8-mm length, REB1-REB2, two boards for specimens of 32-mm length, REB3-REB4, and three boards for specimens of 120-mm length, REB5-REB7, were used. Specimens of 8-mm and 32-mm lengths were cut in two rows from each board, and specimens of 120-mm length were cut in one row, taking into account the geometries of the specimens and boards. In

addition to the regular boards, three boards with randomly positioned specimens of all sizes were used, (see e.g. RAB1 in Fig. 4d).

The following system is used to refer to the specimens in this study: TT-abc-de-fghi where TT refers to transverse tensile, 'abc' is the specimen length in mm (008, 032, 120) and 'de' denotes the specimen ID number in each group of specimens of the same length. Finally, 'fghi' indicates the specific board. For example, TT-120-11-REB5 refers to the specimen number 11, cut from the board REB5 in the transverse direction and has a nominal length of 120 mm. All specimens have the same cross-sectional area of 16 $mm^2$.

*2.3. Clear timber mesostructure*

The mesostructure of the clear spruce wood is mainly characterized by the earlywood-latewood patterns. The main local mesostructural characteristics that can affect the local mechanical properties are shown in Fig. 5. The darker part of each growth ring is latewood that has superior mechanical properties, hereafter called 'strips of latewood' within the cut specimens. In theory, the growth rings are perpendicular to the tree radial direction (radial plane of the tree). However, in practice the local point-by-point tangential direction of the grow rings is not always exactly perpendicular to the corresponding radial plane of the tree, as the grow rings are not perfect circles This fact, along with the natural variability of the timber local structure, such as grow ring thickness, cause the variability in the local mesostructure of the specimens. Figure 5 illustrates the change in the growth ring angle with respect to the loading direction. The local mechanical properties in the loading direction (the radial tree direction) are higher when the angle is closer to 0°, since timber has superior mechanical properties in the radial direction [22]. It can be seen in Fig. 5 that in some growth rings, the latewood thickness is higher than others which also influences the local mechanical properties. Finally, Fig. 5 shows the change in the growth ring thickness; two different growth rings with the same thickness can have different proportions of early- and latewood. These local microstructural variations are the main reasons for the random spatial variability in the local mechanical properties.

*2.4. Experimental set-up and instrumentation*

All experiments were carried out on a 5 kN electromechanical Walter+Bai testing machine, under quasi-static tensile loading in displacement-control mode. Stroke rates for different lengths were selected based on a preliminary testing program, in order to keep the same strain rate in the middle zone of each specimen. Higher stroke rates were applied to longer specimens and lower to shorter specimens to achieve failure within 180 ± 60 s for all lengths.

A video extensometry system composed of a 10-bit Sony XCLU1000 CCD connected to a Fujinon HF35SA-1, 35-mm f 1.4-22 lens with an accuracy of ± 0.005 mm was used during the experiments to measure the axial deformation. Prior to the tests, black target dots of 1.1-mm diameter were applied on the specimens' surfaces. The distance between each two consecutive dots was 4 mm for all groups of specimens. The axial coordinates of the dots were recorded at a frequency of 5 Hz by the video extensometer camera throughout loading. Using these data, the engineering strain between each two consecutive dots was calculated, designated as the local strain. These data were used for calculation of the local elastic modulus, $E_{loc}$. Similarly, based on the displacements of the first and last dots on each specimen, an overall strain for each nominal length was obtained. The overall strains were used for plotting the stress-strain curves presented in this work. Load measurements were divided by the initial cross-sectional area to obtain nominal axial stresses during tests. The effective elastic modulus, $E_{eff}$, for each specimen was estimated from the slope of a linear fit to the entire stress-strain curve of that specimen.

## 3. Experimental results

### *3.1 Stress-strain curves and length effect on strength*

The mechanical properties of each specimen including the effective elastic modulus, the strength and the strain to failure as well as their maximum and minimum values in each board, along with density and failure mode, are given in Tables 1-3. Mean values and COVs are given in Table 4.

Stress-strain curves for the 8-mm-, 32-mm- and 120-mm-length specimens, cut from the REBs, are shown in Figs. 6-8, respectively. In the cases of boards with two rows of specimens (specimens of 8 and 32 mm length), the curves in each row are shown by two different colors. Maximum and minimum strengths and strain to failure are indicated by vertical and horizontal dashed lines in each figure.

An almost linear stress-strain behavior is observed for most of the specimens. The scatter in the effective elastic modulus, strength and strain to failure (overall strain) is high for all specimen series. In a few cases, the minimum strength was observed for the specimen that attained also the minimum strain to failure, especially when the strength of one specimen in a board is distinctly lower than the average strength of all specimens from that same board.

Considering specimens of 8 mm length, the results for the two rows of REB1 or REB2 are not significantly different, as seen in Fig. 6 and Table 4. Specimens cut from REB1 have slightly higher strengths but slightly lower elastic modulus, nevertheless, their strength variation is lower compared to the variation of the specimens cut from REB2.

The specimens of 32 mm length cut from REB3 in the upper row exhibit higher moduli and strengths and lower strains to failure compared to the specimens in the lower row. In REB4, however, the results from the specimens from the two rows are not significantly different. Consequently, the overall variability in the mechanical properties is higher in REB3. In average, the specimens from REB3 are less stiff and less strong, but reaching higher strains to failure, compared to specimens from REB4. Specimens from REB3 with higher moduli are those having the higher strength as well, which is not the case in REB4.

The mechanical properties of the 120 mm specimens from each board (REB5-REB7), are significantly different from those of specimens from the other boards. The specimens from REB5 show lower values for moduli and strengths, but higher scatter in the effective elastic modulus and strain to failure. REB6 shows higher scatter in the strength. REB7 has the lowest scatter in all the properties. These results show a significant board-to-board variability; the mechanical properties change from one specimen to another. In addition, the average mechanical properties of boards are also different. To visualize the board-to-board variability, Figs. 9 and 10 show the effective elastic modulus, and the coefficient of variation of the local elastic modulus within each specimen, for all tested specimens in REB5-REB7. Specimen number in x-axis correspond to the number of each 120 mm long specimen cut from the corresponding REB board, see Table 3. This shows that the properties' variability estimated by specimens cut from one board might not be representative. Consequently, when investigating of the size effect, specimens of different sizes should be cut randomly from multiple boards, eliminating this way the board-to-board variability.

Comparing the results for specimens of different lengths given in Table 4, it can be observed that specimens of 8 mm length exhibit a lower variability in their mechanical properties. Due to their small length, specimens in each row represent mainly the variability of the mechanical properties in the longitudinal direction, since they are cut at the same radial position. The variability of the transverse elastic modulus in the radial direction of the boards can be investigated more efficiently when specimens are longer. Also, the strength values are generally higher for specimens of shorter lengths, indicating a size effect on the strength, as was also observed for the longitudinal strength of the same material in [4].

The experimental results for the mechanical properties of specimens of different lengths from RAB1-RAB3 are shown in Fig. 11. The mechanical behavior is reasonably linear, similar to the REBs. The strength consistently decreases with increasing specimen length. The scatter of the overall elastic moduli is much higher for the specimens with 8 mm length, compared to results from REBs, due to the fact that these specimens are randomly positioned within boards, and radial variability is also present. The scatter in the effective elastic modulus reduces, as the size increases.

Mean strengths and the strength variations between the RAB boards versus specimen length are shown in Fig. 12. The experimental data show a linear decreasing trend on the logarithmic scale, in accordance with the classical Weibull size effect law (CWSEL) [4], although it has been shown elsewhere [4, 23], that the CWSEL is not an appropriate model to simulate the longitudinal strength of clear spruce at mesoscale. The slope of this line depends on the shape factor of the corresponding Weibull distribution, which is a function of only the coefficient of variation (COV). The COVs of the strength data for specimens of 8, 32 and 120 mm lengths are 10.9%, 13.4% and 10.5%, respectively. An average COV was used to obtain a slope of -0.095 for this set of data. Examining the accuracy of CWSEL for specimens cut from REBs would be incorrect since it would violate the basic assumption of the CWSEL that COV should not change with changing specimen size from one group to another [23]. In this experimental program, the COV of the set of all 8 mm specimens in REBs was calculated to 8.14%, being less than half of the corresponding value of 17.66% for 32 mm specimens. This is because in REB1-REB2 strengths are only measured along narrow longitudinal strips of 8 mm width, therefore they show significantly lower variability when compare to 32 mm specimens for which the strips are 4 times wider. In other words, the effect of change of measurement position in the transverse direction on the COV of strength is lowered to a significant degree for 8 mm specimens in REB1-REB2. Consequently, specimens within this group are not appropriate for analysis by using the Weibull theory of size effect.

### *3.2 Correlations between elastic modulus, strength and density*

Fig. 13 shows the tensile strength of each specimen vs the corresponding local elastic modulus measured at the failure zone. The data from each of the specimen groups are indicated by a different symbol. The centroid of each group is indicated by a larger symbol of the same type. Since the correlation between local properties is considered, all specimen strengths and their

corresponding local modulus can be used for estimation of a single correlation coefficient. Both mean local elastic moduli and mean strengths decrease as length increases. The linear correlation coefficient was estimated to 0.61 by MATLAB, which is considered as a moderate correlation. A correlation coefficient of less than 0.4 is considered as a weak correlation. Correlation coefficient of 1 defines a deterministic correlation between the two property values.

The scatter plot of specimens' effective elastic modulus versus their densities is shown in Fig. 14. There is no significant correlation in this case. One reason for this is that the effect of the deviation angle on the variability of the effective elastic modulus is more significant than that of the density, as is shown in the next section. These results are compatible with observations in [24] where no consistent correlation between density and transverse elastic parameters was reported.

The scatter plot of the specimens' strengths versus their densities is shown in Fig. 15, and a relatively weak correlation of 0.21 was estimated in this case. When 10 outlier data points, specified by a dashed box in Fig.15, are excluded, the correlation increases to 0.34, which is still a weak correlation. This is expected as the strength is affected significantly by the local specimen microstructure. Therefore, strength measurements should be correlated to local density (at the position of failure), nevertheless, such measurements were not performed during this study.

Regression lines were also plotted in Fig. 13 to 15. Nevertheless, except from that shown in Fig. 13, those in Figs. 14 and 15 are of low importance since the correlation of the data shown in these two figures is very low. Especially for the case of Fig. 14, the regression line has a negative slope, implying a reduction of stiffness with increasing density, something that is not supported by the available experimental evidence for these materials, showing that the modulus usually increases with density. It is intuitively concluded from this result that only a weak correlation exists between the specimens' density and their effective elastic modulus .

Strength and local elastic modulus have the highest correlation value. One reason is that both are local parameters. The correlation between strength and density compared to that between stiffness and density is higher due to the lower variability of strength compared to the variability of the effective elastic modulus. The effect of density and deviation on the strength are comparable. However, the deviation angle variation is the main reason for the effective elastic modulus variability, and probably overshadows the density effect on the effective elastic modulus.

## 4. Discussion

### *4.1 Effect of timber mesostructure on mechanical properties*

The local mesostructure of clear timber affects the mechanical properties. Characteristic examples of the local mesostructure effect on the specimen local elastic modulus are presented in Fig. 16, for three specimens of 120 mm length.

For specimen TT-120-11-REB5, the deviation angle decreases from left to right with exception to the region between 70 - 95 mm. These angle fluctuations are reflected in the local elastic modulus measurements. As the deviation angle decreases, the elastic modulus increases, while as the deviation angle increases (in the region between 70 - 95 mm) the elastic modulus decreases again. The maximum elastic modulus is measured at the end of the specimen (at 120 mm) where the deviation angle is the minimum. The localized decrease of the elastic modulus in the segment between 110 mm and 115 mm is attributed to a decrease in the thickness of the latewood strips in this zone. The variation of the elastic modulus is very significant. The local elastic modulus ranges between approximately 0.2 GPa and 1 GPa, within a single specimen. Incorporating this variation in the local elastic modulus into finite element simulations of components such as timber joints, definitely leads to a different stress field compared to the case where this variation is neglected. This, in turn, leads to a different probability of failure under external loading. Therefore, accurate modeling of timber structures entails incorporation of local variability of the elastic modulus. However, this variability has been mostly neglected in the literature [3, 17, 18].

A decrease in the deviation angle can be observed over the first 10 mm of specimen TT-120-36-REB6. Then from 10 mm to about 60 mm the deviation angle increases and after that decreases. Correspondingly, the value of the elastic modulus first increases, then decreases and finally increases again. The effect of the deviation angle on the local elastic modulus is also clear at the last 20 mm of the specimen length. In this segment of the specimen, the deviation angle initially increases and then decreases, while, accordingly, there is a localized minimum for the local elastic modulus in the middle of this segment. Another local maximum for the local elastic modulus appears at about 80 mm where the deviation angle has a local minimum in this position of the specimen. In this specimen, the local elastic modulus changes roughly from 0.5 GPa to 1.4 GPa.

Same conclusions can be deduced by observing the specimen mesostructure and the corresponding elastic modulus fluctuations of the TT-120-47-REB7. This specimen shows higher elastic modulus compared to the other two specimens, since it shows a more consistent patterns with small deviation angle. This specimen has thicker latewood strips than the other two specimens, and this could be another reason for the higher measured elastic modulus. Higher volume fractions of, e.g. thicker, or more in an area, latewood strips, increase the local elastic modulus. Both specimens TT-120-11-REB5 and TT-120-47-REB7 show this, having more latewood strips between 60 - 80 mm than anywhere else and therefore, showing higher local elastic modulus in that region.

*4.2 Specimen failures*

Four failure modes have been observed in the specimens, as shown in Fig. 17 where characteristic (side view) photos of failed specimens are presented. The first failure mode, observed in specimens failed within the earlywood, showing an almost perpendicular to the loading/radial direction failure plane. The second failure mode occurs in both earlywood and at growth ring borders (border between the earlywood and the latewood of the previous growth ring) with the failure plane mostly appearing along the local radial bonds. Growth ring border failures occur in the ring border between earlywood and latewood, with oblique, with respect to the cross section, failure plane. The specimens exhibiting the last failure mode, show failure planes approximately perpendicular to the loading direction with failure paths crossing the ring border.

The statistics of strength of all specimens from the REBs and the RABs, grouped according to their failure modes, are given in Table 5. As the deviation angle increases from the first to the fourth mode, the mean strength decreases accordingly, since timber is stronger in the local radial direction than in the local tangential direction [22]. The mean local elastic modulus, at the failure zone, also decreases accordingly.

*4.3 Effects of defects*

Although the investigation focused on clear spruce wood, structural imperfections, such as knots or resin reach areas (resin checks), were present near or within very few of the examined specimens. Figure 18a and b show the lower part of specimen TT-120-05-REB5 after failure, where a small knot is present over the first 16 mm of the specimen length. The location on the board is indicated in Fig. 4c with a rectangle at the lower left area of the board. In this area, the local elastic modulus was much higher than that of the other specimens in the board. The value

of the local elastic modulus at the first 4 mm segment of this specimen was more than six times higher than the maximum value of local elastic modulus at the same radial position for other specimens in REB5. Although there was a crack near the first black dot, the failure occurred in the middle of the specimen supporting the conjecture that the area around the knot can be stronger than the rest of the specimen.

Even small knots can affect the adjacent clear wood mesostructure. A knot has been observed in REB5 as shown in Fig. 4c (specified by a rectangle on the right side of the board). A zoom to the area around that knot is shown in Fig. 19, with the exact knot location indicated by a circle. As shown, the presence of the knot causes waviness of the grains at the longitudinal direction. The specimen with the knot and the one to the left were broken during fabrication and were discarded. However, the specimens TT-120-15-REB5 (further left) and TT-120-16-REB5, (to the right) are shown in Fig. 19, have different microstructure, especially in the range between 75-100 mm. Side view of both specimens is shown in Fig. 20, showing the difference between specimen TT-120-15-REB5 and TT-120-16-REB5. Specimen TT-120-14-REB5 located left from specimen TT-120-15-REB5, therefore further away from the knot is also added to Fig. 20. Since it is away from the knot it shows similar mesostructure with specimen TT-120-15-REB5.

Fig. 21 shows specimen TT-120-59-RAB2 having several knots along its length. The effective elastic modulus and the density of this specimen were 1214.7 MPa and 577.2 kg/m$^3$. Compared to the mean modulus and the mean density of the rest of 120 mm specimens in RAB2, the corresponding values of this specimen are, respectively, 69.9 % and 35.1 % higher. The failure occurred at a knot-free area and the strength was 8.84 MPa which does not show a noticeable deviation from other 120 m specimens in the same board. In practice, the knots affect the structural response depending on their type, the type and direction of loading, their location etc. Although the knots are usually stronger than the clear wood, in some cases, however, the different characteristics of the know and the surrounding area compared to the clear timber (higher stiffness, different thermal and moisture expansion coefficients etc) can create cracks in the interface between the knot and the surrounding clear wood, and therefore the entire knot area is weak. This is the main reason that the knots are avoided as much as possible in wooden structures. A higher number of knots in a structure increases the possibility of the presence of weak areas in a structure.

The only specimen with a resin check (TT-032-02-REB3) is shown in Fig. 22, after failure. The cross section of this specimen in the position of the resin check is also shown to the right

of the specimen, which is outside the nominal length. The strength of this specimen was very low, 2.48 MPa, compared to the average of the strengths of the two neighboring specimens which was 8.89 MPa. Therefore, the crack caused by the resin check reduced the strength by approximately 72.1%.

## 5. Conclusions

In this study, an experimental campaign including transverse tensile quasi-static tests on specimens of different lengths made of clear spruce wood was conducted. A total number of 226 valid experimental results were obtained. The cross-sectional area was the same for all specimens and reasonably small, in order to exclude the effect of the variability of the properties in the cross section. The nominal length of specimens varied from 8 mm to 120 mm in order to investigate the size effect on the mechanical properties. The following main conclusions were drawn:

- A high level of statistical variability was observed in the effective transverse elastic modulus of clear spruce wood. This variability decreases as specimen length increases. The specimens' mean strength decreases as well with increasing length. These observations indicate the existence of size effects at the mesoscale for clear spruce wood. Unlike for longitudinal strength, the CWSEL is valid for transverse strengths at mesoscale.
- A spatial variability of the mechanical properties was also observed; strength and elastic modulus of specimens cut from different radial positions can be much different.
- Four failure modes were observed, all affected by the wood mesostructure. The strengths, as well as the local elastic moduli, were higher when the deviation angle was lower at the failure zone.
- A qualitative correlation between the local mesostructure and the local transverse elastic modulus was observed. Irregular changes of the wood mesostructured cause the spatial variability of the local elastic modulus. The change in the angle between the local tangential direction and the axis of the specimen is the most important factor influencing the local elastic modulus.
- The wood mesostructure is affected by the presence of knots and therefore the local mechanical properties, at mesoscale, on and around knots are significantly affected.

With recent progress in computational power, stochastic analyses of timber structures are receiving more attention. The results of this work can be used for taking into account the statistical variability of the transverse mechanical properties and their correlations, especially when local mechanical properties are concerned. This is of paramount importance in applications such as adhesively-bonded timber joints, where the transverse mechanical properties play a critical role in determining the load-bearing capacity of the structure, and the failure starts at a localized zone.

**Acknowledgement**

The authors wish to acknowledge the funding of this work through the National Research Program NRP 66 of the Swiss National Science Foundation (Grant No. 406640-136680).

**References**

1. Barrett, J.D., 1974. Effect of size on tension perpendicular-to-grain strength of Douglas-fir. Wood and Fiber 6, 126-143.
2. Dinwoodie, J.M., 2000. Timber: Its nature and behaviour. Taylor & Francis Group.
3. Tannert, T., Lam, F., Vallée, T., 2010. Strength prediction for rounded dovetail connections considering size effects. Journal of Engineering Mechanics 136, 358-366.
4. Moshtaghin, A.F., Franke, S., Keller, T., Vassilopoulos, A.P., 2016. Experimental characterization of longitudinal mechanical properties of clear timber: Random spatial variability and size effects. Construction and building materials 120, 432-441.
5. Forest Product Laboratory, 1999. Wood handbook: Wood as an engineering material, USDA, Madison, Wis, USA.
6. Clouston, P.L., Lam, F., 2002. A stochastic plasticity approach to strength modeling of strand-based wood composites. Composites Science and Technology 62, 1381-1395.
7. Clouston, P.L., Lam, F., 2001. Computational modeling of strand-based wood composites. Journal of Engineering Mechanics 127, 844-851.
8. Arwade, S.R., Clouston, P.L., Winans, R., 2009. Measurement and stochastic computational modeling of the elastic properties of parallel strand lumber. Journal of Engineering Mechanics 135, 897-905.

9. Zhu, J., Kudo, A., Takeda, T., Tokumoto, M., 2001. Methods to estimate the length effect on tensile strength parallel to the grain in Japanese larch. Journal of Wood Science 47, 269-274.
10. Dill-Langer, G., Hidalgo, R.C., Kun, F., Moreno, Y., Aicher, S., Herrmann, H.J., 2003. Size dependency of tension strength in natural fiber composites. Physica A: Statistical Mechanics and its Applications 325, 547-560.
11. Siegel, C., Buchelt, B., Wagenführ, A., 2020. Application of the three-point bending test for small-sized wood and veneer samples. Wood Material Science and Engineering. DOI: 10.1080/17480272.2020.1814410
12. Barrett, J.D., Foschi, R.O., Fox, S.P., 1975. Perpendicular-to-grain strength of Douglas-Fir. Canadian Journal of Civil Engineering 2, 50-57.
13. Fox, S.P., 1974. Strength and stiffness of laminated Douglas-fir blocks in perpendicular-to-glueline tension. Wood and Fiber 6, 156-163.
14. Norlin, L.P., Lam, F., 1998. Fatigue behaviour and size effects perpendicular to the grain of laminated Douglas fir veneer. Materials and structures 32, 298-303.
15. Pedersen, M.U., Clorius, C.O., Damkilde, L., Hoffmeyer P., 2003. A simple size effect model for tension perpendicular to the grain. Wood Science and Technology 37, 125-140.
16. Astrup, T., Clorius, C.O., Damkilde, L., Hoffmeyer P., 2007. Size effect of glulam beams in tension perpendicular to grain. Wood Science and Technology 41, 361-372.
17. Tannert, T., Vallée, T., Hehl, S., 2012. Probabilistic strength prediction of adhesively bonded timber joints. Wood Science and Technology 46, 503-513.
18. Tannert, T., Vallée, T., Hehl, S., 2012. Experimental and numerical investigations on adhesively bonded timber joints. Wood Science and Technology 46, 579-590.
19. EN-408, 2012. Timber structures – Structural timber and glued laminated timber – Determination of some physical and mechanical properties.
20. ASTM D143-14, Standard Test Methods for Small Clear Specimens of Timber.
21. Ramage, M.H. et al., 2017. The wood from the trees: The use of timber in construction. Renewable and Sustainable Energy Reviews 68, 333-359.
22. Backman, A.C., Lindberg, K.A.H., 2001. Differences in wood material responses for radial and tangential direction as measured by dynamic mechanical thermal analysis. Journal of Materials Science 36, 3777-3783.

23. Moshtaghin, A.F., Franke, S., Keller, T., Vassilopoulos, A.P., 2016. Random field-based modeling of size effect on the longitudinal tensile strength of clear timber. Structural Safety 58, 60-68.
24. Pereira, J., Xavier J., Morais J., Lousada J., 2014. Assessing wood quality by spatial variation of elastic properties within the stem: Case study of Pinus pinaster in the transverse plane. Canadian Journal of Forest Research 44, 107-117.

**Table 1.** Effective elastic modulus, strength, strain to failure, density and failure mode for 8-mm specimens.

| Specimen code | Effective E (MPa) | Strength (MPa) | Strain to failure (%) | Density (kg/m$^3$) | Failure mode | Maxima and minima |
|---|---|---|---|---|---|---|
| TT-008-01-REB1 | 735.8 | 9.97 | 1.35 | 442.4 | 3 | Max(E)=1184.3 MPa |
| TT-008-02-REB1 | 655.1 | 10.2 | 1.56 | 452.4 | 3 | Min(E)=643.3 MPa |
| TT-008-03-REB1 | 643.3 | 9.61 | 1.49 | 464.3 | 1 | Max(S)=10.59 MPa |
| TT-008-04-REB1 | 918.0 | 7.01 | 0.76 | 458.4 | 1 | Min(S)=7.01 MPa |
| TT-008-05-REB1 | 837.8 | 10.40 | 1.24 | 452.5 | 1 | Max(ε)=1.56 % |
| TT-008-06-REB1 | 664.4 | 9.82 | 1.48 | 441.4 | 3 | Min(ε)=0.75 % |
| TT-008-07-REB1 | 970.8 | 9.77 | 1.01 | 459.0 | 1 | |
| TT-008-08-REB1 | 667.6 | 9.073 | 1.36 | 453.4 | 3 | |
| TT-008-09-REB1 | 723.5 | 9.52 | 1.32 | 465.6 | 1 | |
| TT-008-10-REB1 | 676.1 | 9.80 | 1.45 | 472.7 | 1 | |
| TT-008-11-REB1 | 681.6 | 10.06 | 1.46 | 462.4 | 1 | |
| TT-008-12-REB1 | 868.7 | 10.19 | 1.17 | 466.5 | 1 | |
| TT-008-13-REB1 | 722.4 | 10.59 | 1.47 | 465.8 | 1 | |
| TT-008-14-REB1 | 676.8 | 10.09 | 1.49 | 461.3 | 1 | |
| TT-008-15-REB1 | 818.7 | 9.84 | 1.20 | 409.3 | 1 | |
| TT-008-16-REB1 | 672.9 | 9.52 | 1.41 | 409.7 | 1 | |
| TT-008-17-REB1 | 737.7 | 9.50 | 1.29 | 418.0 | 1 | |
| TT-008-18-REB1 | 759.7 | 9.20 | 1.21 | 405.3 | 2 | |
| TT-008-19-REB1 | 893.9 | 9.17 | 1.03 | 402.6 | 2 | |
| TT-008-20-REB1 | 881.6 | 9.64 | 1.09 | 426.4 | 1 | |

| | | | | | | |
|---|---|---|---|---|---|---|
| TT-008-21-REB1 | 868.7 | 9.31 | 1.07 | 421.2 | 1 | |
| TT-008-22-REB1 | 712.1 | 9.61 | 1.35 | 417.0 | 1 | |
| TT-008-23-REB1 | 655.5 | 9.43 | 1.44 | 423.1 | 1 | |
| TT-008-24-REB1 | 677.7 | 9.09 | 1.34 | 421.2 | 2 | |
| TT-008-25-REB1 | 720.4 | 9.67 | 1.34 | 415.4 | 1 | |
| TT-008-26-REB1 | 798.3 | 9.84 | 1.23 | 417.5 | 1 | |
| TT-008-27-REB1 | 1184.3 | 8.90 | 0.75 | 424.2 | 1 | |
| TT-008-28-REB2 | 597.7 | 8.90 | 1.49 | 458.9 | 1 | Max(E)=1121.4 MPa |
| TT-008-29-REB2 | 754.9 | 10.75 | 1.42 | 455.1 | 1 | Min(E)=575.2 MPa |
| TT-008-30-REB2 | 748.4 | 10.60 | 1.42 | 459.5 | 1 | Max(S)=10.75 MPa |
| TT-008-31-REB2 | 755.2 | 9.02 | 1.19 | 455.1 | 1 | Min(S)=8.07 MPa |
| TT-008-32-REB2 | 642.3 | 9.40 | 1.46 | 453.2 | 1 | Max(ε)=1.49 % |
| TT-008-33-REB2 | 707.7 | 8.62 | 1.22 | 458.4 | 1 | Min(ε)=0.87 % |
| TT-008-34-REB2 | 917.5 | 9.62 | 1.05 | 459.6 | 1 | |
| TT-008-35-REB2 | 1121.4 | 10.69 | 0.95 | 454.3 | 1 | |
| TT-008-36-REB2 | - | 10.37 | - | 544.1[*2] | 1 | |
| TT-008-37-REB2 | 1003.8 | 8.74 | 0.87 | 449.8 | 1 | |
| TT-008-38-REB2 | 803.9 | 8.47 | 1.05 | 449.5 | 1 | |
| TT-008-39-REB2 | 827.1 | 9.66 | 1.17 | 446.1 | 1 | |
| TT-008-40-REB2 | 899.9 | 9.26 | 1.03 | 441.9 | 1 | |
| TT-008-41-REB2 | 869.8 | 9.34 | 1.07 | 446.5 | 1 | |
| TT-008-42-REB2 | 911.3 | 9.27 | 1.02 | 430.8 | 1 | |
| TT-008-43-REB2 | 906.7 | 8.54 | 0.94 | 437.8 | 1 | |
| TT-008-44-REB2 | 850.3 | 8.50 | 1.00 | 441.9 | 1 | |
| TT-008-45-REB2 | 763.0 | 8.27 | 1.08 | 430.9 | 1 | |
| TT-008-46-REB2 | 838.4 | 8.53 | 1.02 | 430.1 | 1 | |
| TT-008-47-REB2 | 673.2 | 8.07 | 1.20 | 429.0 | 1 | |

[*] Specimen densities affected by a nearby knot (mainly in tab of the specimen) are indicated by * and are excluded from further analyses.

| | | | | | | |
|---|---|---|---|---|---|---|
| TT-008-48-REB2 | 575.2 | 8.14 | 1.42 | 430.1 | 1 | |
| TT-008-49-RAB1 | 559.0 | 9.70 | 1.74 | 458.4 | 1 | Max(E)=773.5 MPa |
| TT-008-50-RAB1 | 598.3 | 9.68 | 1.62 | 453.5 | 1 | Min(E)=251.9 MPa |
| TT-008-51-RAB1 | 773.5 | 10.91 | 1.41 | 446.4 | 1 | Max(S)=10.91 MPa |
| TT-008-52-RAB1 | 358.9 | 8.71 | 2.43 | 457.3 | 1 | Min(S)=8.10 MPa |
| TT-008-53-RAB1 | 595.4 | 9.86 | 1.66 | 454.6 | 1 | Max(ε)=3.46 % |
| TT-008-54-RAB1 | 482.8 | 8.10 | 1.68 | 451.5 | 2 | Min(ε)=1.41 % |
| TT-008-55-RAB1 | 251.9 | 8.72 | 3.46 | 462.7 | 1 | |
| TT-008-56-RAB1 | 279.2 | 8.19 | 2.93 | 443.7 | 4 | |
| TT-008-57-RAB1 | 329.5 | 8.15 | 2.47 | 424.5 | 3 | |
| TT-008-58-RAB2 | 839.8 | 10.00 | 1.19 | 407.1 | 1 | Max(E)=773.5 MPa |
| TT-008-59-RAB2 | 746.1 | 10.51 | 1.41 | 442.8 | 1 | Min(E)=251.9 MPa |
| TT-008-60-RAB2 | 438.0 | 9.60 | 2.19 | 439.7 | 1 | Max(S)=11.53 MPa |
| TT-008-61-RAB2 | 940.0 | 11.53 | 1.23 | 455.1 | 1 | Min(S)=9.60 MPa |
| TT-008-62-RAB2 | 645.5 | 9.67 | 1.50 | 439.9 | 1 | Max(ε)=3.46 % |
| TT-008-63-RAB2 | 892.7 | 11.05 | 1.24 | 446.1 | 1 | Min(ε)=1.41 % |
| TT-008-64-RAB2 | 793.5 | 10.91 | 1.37 | 454.6 | 2 | |
| TT-008-65-RAB2 | 765.4 | 11.46 | 1.50 | 547.0* | 1 | |
| TT-008-66-RAB3 | 733.8 | 9.73 | 1.33 | 473.7 | 3 | Max(E)=734.5 MPa |
| TT-008-67-RAB3 | 393.9 | 8.03 | 2.04 | 424.3 | 1 | Min(E)=312.7 MPa |
| TT-008-68-RAB3 | 719.6 | 9.44 | 1.31 | 455.6 | 1 | Max(S)=11.17 MPa |
| TT-008-69-RAB3 | 734.5 | 9.72 | 1.32 | 446.9 | 3 | Min(S)=8.03 MPa |
| TT-008-70-RAB3 | 418.1 | 8.46 | 2.02 | 459.5 | 3 | Max(ε)=2.89 % |
| TT-008-71-RAB3 | 312.7 | 9.05 | 2.89 | 455.0 | 1 | Min(ε)=1.31 % |
| TT-008-72-RAB3 | 380.0 | 9.57 | 2.52 | 461.3 | 1 | |
| TT-008-73-RAB3 | 458.2 | 9.56 | 2.09 | 455.5 | 1 | |
| TT-008-74-RAB3 | 426.1 | 11.17 | 2.62 | 462.4 | 1 | |
| TT-008-75-RAB3 | 649.6 | 10.61 | 1.63 | 446.5 | 1 | |

**Table 2.** Effective elastic modulus, strength, strain to failure, density and failure mode for 32-mm specimens.

| Specimen code | Effective E (MPa) | Strength (MPa) | Strain to failure (%) | Density (kg/m$^3$) | Failure mode | Maxima and Minima |
|---|---|---|---|---|---|---|
| TT-032-01-REB3 | 597.6 | 8.97 | 1.50 | 438.2 | 1 | Max(E)=674.8 MPa |
| TT-032-02-REB3 | 538.2 | 2.48 | 0.46 | 455.0 | 4 | Min(E)=104.3 MPa |
| TT-032-03-REB3 | 674.8 | 8.81 | 1.31 | 450.5 | 1 | Max(S)=9.60 MPa |
| TT-032-04-REB3 | 441.3 | 8.58 | 1.94 | 446.9 | 1 | Min(S)=2.48 MPa |
| TT-032-05-REB3 | 406.6 | 8.03 | 1.97 | 445.1 | 1 | Max(ε)=5.42 % |
| TT-032-06-REB3 | 408.7 | 8.49 | 2.08 | 444.4 | 1 | Min(ε)=0.46 % |
| TT-032-07-REB3 | 362.6 | 8.44 | 2.33 | 448.3 | 4 | |
| TT-032-08-REB3 | 385.1 | 9.60 | 2.49 | 490.2 | 1 | |
| TT-032-09-REB3 | 477.5 | 8.07 | 1.69 | 450.0 | 1 | |
| TT-032-10-REB3 | 168.7 | 6.26 | 3.71 | 435.9 | 1 | |
| TT-032-11-REB3 | 154.5 | 6.48 | 4.20 | 443.5 | 4 | |
| TT-032-12-REB3 | 130.7 | 5.99 | 4.58 | 447.2 | 1 | |
| TT-032-13-REB3 | 105.9 | 5.08 | 4.80 | 448.3 | 1 | |
| TT-032-14-REB3 | 104.3 | 5.65 | 5.42 | 435.7 | 3 | |
| TT-032-15-REB3 | 126.0 | 5.58 | 4.43 | 431.1 | 4 | |
| TT-032-16-REB3 | 144.6 | 5.82 | 4.02 | 442.1 | 4 | |
| TT-032-17-REB3 | 162.3 | 6.72 | 4.14 | 436.5 | 1 | |
| TT-032-18-REB3 | 181.2 | 6.82 | 3.76 | 419.4 | 1 | |
| TT-032-19-REB3 | 248.4 | 6.58 | 2.65 | 443.6 | 3 | |
| TT-032-20-REB3 | 323.0 | 7.71 | 2.39 | 439.9 | 1 | |
| TT-032-21-REB4 | 295.5 | 8.31 | 2.81 | 447.8 | 1 | Max(E)=923.7 MPa |
| TT-032-22-REB4 | 407.8 | 6.46 | 1.58 | 453.1 | 2 | Min(E)=295.5 MPa |
| TT-032-23-REB4 | 443.5 | 7.68 | 1.73 | 435.5 | 3 | Max(S)=9.98 MPa |
| TT-032-24-REB4 | 448.4 | 8.06 | 1.80 | 436.1 | 1 | Min(S)=6.46 MPa |
| TT-032-25-REB4 | 422.9 | 7.37 | 1.74 | 436.5 | 3 | Max(ε)=2.81 % |
| TT-032-26-REB4 | 462.4 | 8.08 | 1.75 | 431.2 | 1 | Min(ε)=0.86 % |

| | | | | | | |
|---|---|---|---|---|---|---|
| TT-032-27-REB4 | 536.4 | 7.50 | 1.40 | 438.9 | 3 | |
| TT-032-28-REB4 | 710.8 | 7.66 | 1.08 | 441.4 | 3 | |
| TT-032-29-REB4 | 778.5 | 6.66 | 0.86 | 405.8 | 2 | |
| TT-032-30-REB4 | 667.0 | 8.15 | 1.22 | 433.1 | 1 | |
| TT-032-31-REB4 | 824.3 | 8.54 | 1.04 | 436.7 | 3 | |
| TT-032-32-REB4 | 923.7 | 8.84 | 0.96 | 439.2 | 1 | |
| TT-032-33-REB4 | 304.3 | 6.98 | 2.29 | 451.5 | 1 | |
| TT-032-34-REB4 | 344.2 | 7.60 | 2.21 | 443.5 | 1 | |
| TT-032-35-REB4 | 348.9 | 8.02 | 2.30 | 469.1 | 1 | |
| TT-032-36-REB4 | 472.5 | 8.20 | 1.74 | 442.1 | 1 | |
| TT-032-37-REB4 | 491.2 | 8.17 | 1.66 | 434.1 | 1 | |
| TT-032-38-REB4 | 595.1 | 8.09 | 1.36 | 429.3 | 1 | |
| TT-032-39-REB4 | 653.9 | 8.02 | 1.23 | 430.8 | 1 | |
| TT-032-40-REB4 | 743.9 | 8.50 | 1.14 | 429.6 | 1 | |
| TT-032-41-REB4 | 795.1 | 8.21 | 1.03 | 432.0 | 1 | |
| TT-032-42-REB4 | 805.5 | 8.32 | 1.03 | 424.4 | 1 | |
| TT-032-43-REB4 | 669.6 | 8.57 | 1.28 | 443.9 | 1 | |
| TT-032-44-REB4 | 813.5 | 9.98 | 1.23 | 468.4 | 1 | |
| TT-032-45-REB4 | 792.9 | 8.52 | 1.07 | 442.8 | 1 | |
| TT-032-46-RAB1 | 928.9 | 9.04 | 0.97 | 434.4 | 1 | Max(E)=928.9 MPa |
| TT-032-47-RAB1 | 867.1 | 9.96 | 1.15 | 438.7 | 1 | Min(E)=321.4 MPa |
| TT-032-48-RAB1 | 537.9 | 9.50 | 1.77 | 451.5 | 3 | Max(S)=9.96 MPa |
| TT-032-49-RAB1 | 428.8 | 8.22 | 1.92 | 449.4 | 3 | Min(S)=4.88 MPa |
| TT-032-50-RAB1 | 519.4 | 9.69 | 1.87 | 438.7 | 1 | Max(ε)=2.61 % |
| TT-032-51-RAB1 | 451.0 | 7.92 | 1.76 | 448.0 | 3 | Min(ε)=0.97 % |
| TT-032-52-RAB1 | 492.3 | 9.52 | 1.93 | 438.3 | 3 | |
| TT-032-53-RAB1 | 321.4 | 8.38 | 2.61 | 439.3 | 3 | |
| TT-032-54-RAB1 | 353.9 | 4.88 | 1.38 | 430.8 | 2 | |
| TT-032-55-RAB2 | 549.0 | 9.93 | 1.81 | 454.6 | 1 | Max(E)=861.5 MPa |

| | | | | | | |
|---|---|---|---|---|---|---|
| TT-032-56-RAB2 | 666.3 | 10.07 | 1.51 | 447.5 | 1 | Min(E)=499.1 MPa |
| TT-032-57-RAB2 | 861.5 | 8.65 | 1.00 | 432.2 | 1 | Max(S)=10.23 MPa |
| TT-032-58-RAB2 | 499.1 | 9.20 | 1.84 | 430.2 | 1 | Min(S)=7.44 MPa |
| TT-032-59-RAB2 | 758.6 | 9.23 | 1.22 | 431.0 | 1 | Max(ε)=1.84 % |
| TT-032-60-RAB2 | 747.0 | 9.03 | 1.21 | 423.7 | 1 | Min(ε)=0.98 % |
| TT-032-61-RAB2 | 811.0 | 9.15 | 1.13 | 442.1 | 1 | |
| TT-032-62-RAB2 | 839.0 | 9.51 | 1.13 | 445.6 | 1 | |
| TT-032-63-RAB2 | 637.5 | 7.86 | 1.23 | 425.1 | 1 | |
| TT-032-64-RAB2 | 662.2 | 8.38 | 1.27 | 404.6 | 2 | |
| TT-032-65-RAB2 | 666.0 | 8.41 | 1.26 | 438.4 | 1 | |
| TT-032-66-RAB2 | 760.0 | 7.44 | 0.98 | 439.3 | 3 | |
| TT-032-67-RAB2 | 755.7 | 10.23 | 1.35 | 458.6 | 1 | |
| TT-032-68-RAB2 | 816.2 | 9.33 | 1.14 | 435.9 | 1 | |
| TT-032-69-RAB3 | 867.5 | 9.28 | 1.07 | 445.1 | 1 | Max(E)=926.4 MPa |
| TT-032-70-RAB3 | 586.8 | 8.10 | 1.38 | 445.5 | 1 | Min(E)=414.0 MPa |
| TT-032-71-RAB3 | 854.0 | 5.39 | 0.63 | 448.1 | 3 | Max(S)=10.26 MPa |
| TT-032-72-RAB3 | 643.5 | 7.89 | 1.23 | 452.2 | 1 | Min(S)=5.39 MPa |
| TT-032-73-RAB3 | 916.5 | 8.35 | 0.91 | 465.6 | 3 | Max(ε)=2.12 % |
| TT-032-74-RAB3 | 926.4 | 9.07 | 0.98 | 449.1 | 1 | Min(ε)=0.63 % |
| TT-032-75-RAB3 | 376.9 | 7.88 | 2.09 | 448.1 | 1 | |
| TT-032-76-RAB3 | 378.6 | 8.01 | 2.12 | 452.3 | 1 | |
| TT-032-77-RAB3 | 847.0 | 9.59 | 1.13 | 439.2 | 1 | |
| TT-032-78-RAB3 | 829.5 | 10.26 | 1.24 | 438.8 | 1 | |
| TT-032-79-RAB3 | 433.4 | 8.09 | 1.87 | 478.2 | 1 | |
| TT-032-80-RAB3 | 740.4 | 8.36 | 1.13 | 446.9 | 3 | |
| TT-032-81-RAB3 | 414.0 | 7.71 | 1.86 | 526.6* | 3 | |
| TT-032-82-RAB3 | 523.0 | 9.65 | 1.85 | 574.1* | 1 | |

**Table 3.** Effective elastic modulus, strength, strain to failure, density and failure mode for 120-mm specimens.

| Specimen code | Effective E (MPa) | Strength (MPa) | Strain to failure (%) | Density (kg/m$^3$) | Failure mode | Maxima and minima |
|---|---|---|---|---|---|---|
| TT-120-01-REB5 | 143.3 | 5.44 | 3.80 | 443.2 | 4 | Max(E)=392.0 MPa |
| TT-120-02-REB5 | 177.2 | 4.87 | 2.75 | 449.7 | 4 | Min(E)=143.3 MPa |
| TT-120-03-REB5 | 155.5 | 4.98 | 3.20 | 447.4 | 4 | Max(S)=5.84 MPa |
| TT-120-04-REB5 | 183.8 | 5.25 | 2.86 | 456.0 | 4 | Min(S)=4.45 MPa |
| TT-120-05-REB5 | 230.0 | 4.90 | 2.13 | 529.7* | 3 | Max(ε)=3.80 % |
| TT-120-06-REB5 | 187.5 | 4.45 | 2.37 | 451.1 | 3 | Min(ε)=1.16 % |
| TT-120-07-REB5 | 187.2 | 4.59 | 2.45 | 436.3 | 4 | |
| TT-120-08-REB5 | 198.4 | 5.07 | 2.56 | 441.7 | 4 | |
| TT-120-09-REB5 | 229.06 | 4.86 | 2.12 | 445.6 | 3 | |
| TT-120-10-REB5 | 246.8 | 5.01 | 2.03 | 448.4 | 3 | |
| TT-120-11-REB5 | 278.4 | 4.70 | 1.69 | 447.9 | 2 | |
| TT-120-12-REB5 | 288.5 | 5.45 | 1.89 | 452.2 | 2 | |
| TT-120-13-REB5 | 336.7 | 5.64 | 1.68 | 449.5 | 2 | |
| TT-120-14-REB5 | 360.8 | 4.85 | 1.34 | 450.0 | 2 | |
| TT-120-15-REB5 | 392.0 | 4.53 | 1.16 | 453.1 | 2 | |
| TT-120-16-REB5 | 375.1 | 5.78 | 1.54 | 446.9 | 2 | |
| TT-120-17-REB5 | 341.2 | 5.69 | 1.67 | 442.5 | 2 | |
| TT-120-18-REB5 | 318.7 | 5.84 | 1.83 | 444.7 | 4 | |
| TT-120-19-REB5 | 348.7 | 5.48 | 1.57 | 446.6 | 2 | |
| TT-120-20-REB5 | 352.8 | 5.25 | 1.49 | 450.3 | 3 | |
| TT-120-21-REB5 | 338.7 | 5.59 | 1.65 | 442.3 | 1 | |
| TT-120-22-REB6 | 655.2 | 4.40 | 0.67 | 411.3 | 2 | Max(E)=802.6 MPa |
| TT-120-23-REB6 | 580.8 | 3.66 | 0.63 | 421.1 | 2 | Min(E)=493.8 MPa |
| TT-120-24-REB6 | 556.1 | 2.01 | 0.36 | 420.2 | 4 | Max(S)=7.56 MPa |
| TT-120-25-REB6 | 570.1 | 6.40 | 1.12 | 416.7 | 1 | Min(S)=2.01 MPa |
| TT-120-26-REB6 | 513.8 | 4.95 | 0.96 | 429.7 | 3 | Max(ε)=1.32 % |
| TT-120-27-REB6 | 493.8 | 5.06 | 1.02 | 437.1 | 2 | Min(ε)=0.36 % |

| | | | | | | |
|---|---|---|---|---|---|---|
| TT-120-28-REB6 | 533.1 | 7.06 | 1.32 | 429.5 | 3 | |
| TT-120-29-REB6 | 510.0 | 4.57 | 0.90 | 429.9 | 2 | |
| TT-120-30-REB6 | 530.2 | 5.39 | 1.02 | 426.5 | 2 | |
| TT-120-31-REB6 | 547.2 | 6.12 | 1.12 | 429.0 | 3 | |
| TT-120-32-REB6 | 603.7 | 7.17 | 1.19 | 452.0 | 2 | |
| TT-120-33-REB6 | 606.9 | 6.72 | 1.11 | 430.8 | 3 | |
| TT-120-34-REB6 | 696.8 | 5.93 | 0.85 | 431.2 | 2 | |
| TT-120-35-REB6 | 743.5 | 6.69 | 0.90 | 437.0 | 1 | |
| TT-120-36-REB6 | 744.7 | 4.81 | 0.65 | 427.6 | 1 | |
| TT-120-37-REB6 | 802.6 | 7.56 | 0.94 | 430.5 | 1 | |
| TT-120-38-REB6 | 793.8 | 5.87 | 0.74 | 427.6 | 1 | |
| TT-120-39-REB6 | 768.2 | 3.95 | 0.51 | 428.3 | 2 | |
| TT-120-40-REB7 | 652.0 | 7.16 | 1.10 | 426.0 | 3 | Max(E)=848.5 MPa |
| TT-120-41-REB7 | 654.5 | 6.59 | 1.01 | 431.2 | mixed | Min(E)=641.2 MPa |
| TT-120-42-REB7 | 641.2 | 6.56 | 1.02 | 439.4 | mixed | Max(S)=7.16 MPa |
| TT-120-43-REB7 | 695.6 | 6.07 | 0.87 | 431.5 | mixed | Min(S)=5.73 MPa |
| TT-120-44-REB7 | 680.3 | 6.47 | 0.95 | 428.1 | 1 | Max(ε)=1.10 % |
| TT-120-45-REB7 | 783.4 | 7.13 | 0.91 | 435.3 | 2 | Min(ε)=0.72 % |
| TT-120-46-REB7 | 784.0 | 6.69 | 0.85 | 429.0 | 2 | |
| TT-120-47-REB7 | 799.4 | 5.73 | 0.72 | 426.3 | 3 | |
| TT-120-48-REB7 | 801.6 | 5.97 | 0.74 | 431.6 | 2 | |
| TT-120-49-REB7 | 848.5 | 6.73 | 0.79 | 439.0 | 2 | |
| TT-120-50-REB7 | 800.4 | 7.10 | 0.89 | 425.7 | 2 | |
| TT-120-51-REB7 | 815.3 | 6.99 | 0.86 | 424.0 | 1 | |
| TT-120-52-REB7 | 842.7 | 6.79 | 0.81 | 433.6 | 2 | |
| TT-120-53-RAB1 | 579.9 | 7.45 | 1.28 | 440.7 | 4 | Max(E)=585.8 MPa |
| TT-120-54-RAB1 | 585.8 | 8.63 | 1.47 | 454.4 | 1 | Min(E)=362.0 MPa |
| TT-120-55-RAB1 | 584.7 | 7.31 | 1.25 | 449.8 | 2 | Max(S)=8.63 MPa |
| TT-120-56-RAB1 | 438.4 | 6.28 | 1.43 | 446.1 | 3 | Min(S)=6.28 MPa |

| | | | | | | |
|---|---|---|---|---|---|---|
| TT-120-57-RAB1 | 408.2 | 7.08 | 1.73 | 444.0 | 3 | Max(ε)=1.95 % |
| TT-120-58-RAB1 | 362.0 | 7.05 | 1.95 | 441.6 | 3 | Min(ε)=1.25 % |
| TT-120-59-RAB2 | 1214.7 | 8.84 | 0.73 | 577.2* | 1 | Max(E)=1214.7 MPa |
| TT-120-60-RAB2 | 740.7 | 8.82 | 1.19 | 433.6 | 1 | Min(E)=663.5 MPa |
| TT-120-61-RAB2 | 759.4 | 7.90 | 1.04 | 424.2 | 1 | Max(S)=8.99 MPa |
| TT-120-62-RAB2 | 694.5 | 8.21 | 1.18 | 424.8 | 1 | Min(S)=6.84 MPa |
| TT-120-63-RAB2 | 663.5 | 8.99 | 1.35 | 425.0 | 1 | Max(ε)=1.35 % |
| TT-120-64-RAB2 | 717.2 | 6.84 | 0.95 | 428.5 | 3 | Min(ε)=0.73 % |
| TT-120-65-RAB3 | 666.0 | 7.82 | 1.17 | 434.5 | 3 | Max(E)=666.0 MPa |
| TT-120-66-RAB3 | 517.1 | 7.43 | 1.44 | 441.0 | 3 | Min(E)=501.5 MPa |
| TT-120-67-RAB3 | 547.2 | 8.29 | 1.51 | 434.9 | 1 | Max(S)=9.03 MPa |
| TT-120-68-RAB3 | 501.5 | 9.03 | 1.80 | 438.2 | 1 | Min(S)=7.43 MPa |
| TT-120-69-RAB3 | 542.0 | 7.45 | 1.37 | 460.2 | 1 | Max(ε)=1.17 % |
| | | | | | | Min(ε)=1.80 % |

**Table 4.** Mean values and COVs of effective elastic modulus, strength and strain to failure for each specimen length in each board.

| Specimen length (mm) | Board | Effective elastic modulus (MPa) | | Strength (MPa) | | Strain to failure (%) | |
|---|---|---|---|---|---|---|---|
| | | Mean | COV(%) | Mean | COV(%) | Mean | COV(%) |
| 8 | REB1 | 771.2 | 16.3 | 9.59 | 6.90 | 1.27 | 16.6 |
| | REB2 | 808.4 | 16.8 | 9.18 | 9.19 | 1.15 | 16.7 |
| | RAB1 | 469.8 | 37.5 | 9.11 | 10.70 | 2.16 | 32.7 |
| | RAB2 | 757.6 | 20.8 | 10.60 | 7.26 | 1.45 | 22.1 |
| | RAB3 | 522.7 | 31.9 | 9.53 | 9.62 | 1.98 | 29.1 |
| 32 | REB3 | 307.1 | 58.1 | 7.01 | 24.30 | 2.99 | 45.0 |
| | REB4 | 590.1 | 32.2 | 8.02 | 8.94 | 1.50 | 33.3 |
| | RAB1 | 544.5 | 39.1 | 8.57 | 18.20 | 1.71 | 28.6 |
| | RAB2 | 716.4 | 15.0 | 9.03 | 9.00 | 1.29 | 20.3 |

| | | | | | | | |
|---|---|---|---|---|---|---|---|
| | RAB3 | 667.0 | 31.7 | 8.40 | 14.0 | 1.39 | 34.2 |
| 120 | REB5 | 270.0 | 30.1 | 5.15 | 8.30 | 2.08 | 31.8 |
| | REB6 | 625.0 | 17.0 | 5.46 | 26.2 | 0.89 | 28.5 |
| | REB7 | 753.8 | 10.2 | 6.61 | 6.91 | 0.89 | 12.6 |
| | RAB1 | 493.2 | 20.7 | 7.30 | 10.5 | 1.52 | 17.9 |
| | RAB2 | 798.3 | 25.9 | 8.27 | 9.87 | 1.07 | 20.2 |
| | RAB3 | 554.8 | 11.7 | 8.00 | 8.39 | 1.46 | 15.7 |

**Table 5.** Statistics of strength for all specimens when grouped according to failure modes and statistics of local elastic modulus at failure zone.

| Failure mode | Number of specimens | Mean strength (MPa) | Mean local elastic modulus (MPa) |
|---|---|---|---|
| 1 | 134 | 8.85±1.26 | 634.1±246.1 |
| 2 | 42 | 7.42±1.58 | 614.1±284.9 |
| 3 | 32 | 6.34±1.71 | 546.2±308.6 |
| 4 | 15 | 5.50±1.77 | 179.0±119.0 |

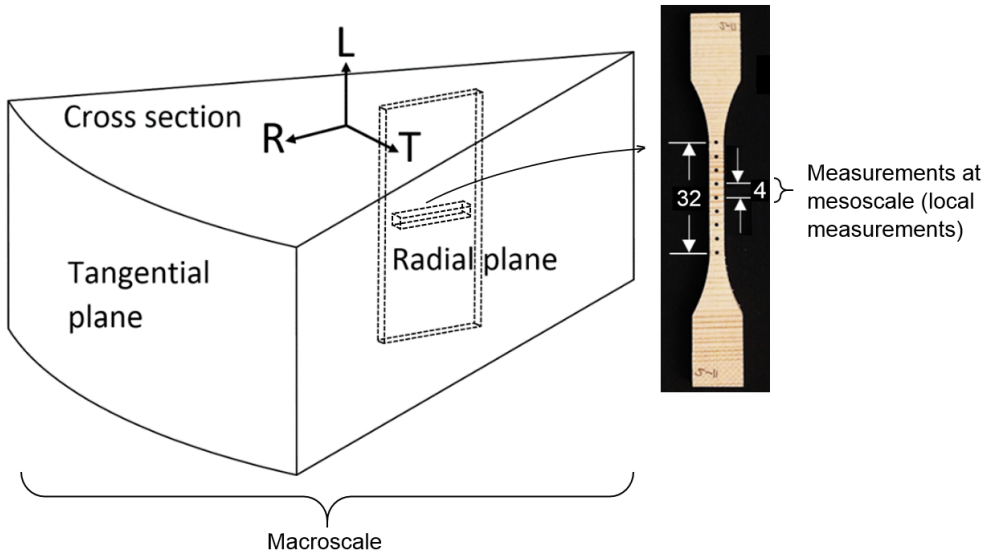


**Fig. 1.** Schematic illustration showing the principal directions, planes, and approximate position of boards (not in scale). Dimensions in mm.

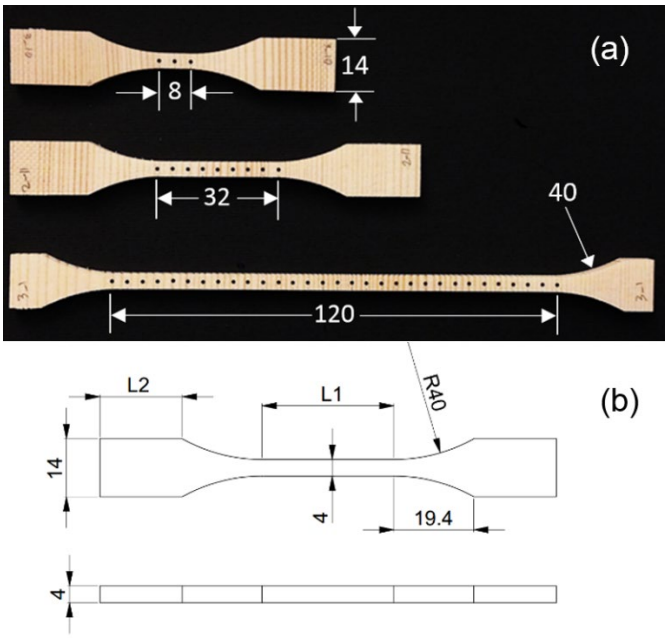


**Fig. 2.** a) Fabricated specimens of different lengths. b) Designed geometry of specimens for transverse tensile tests. Dimensions are in mm.

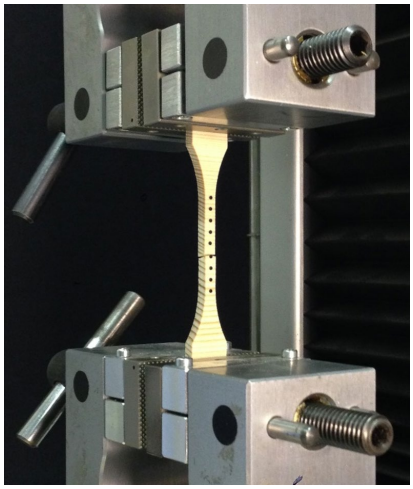

**Fig. 3.** Specimen of 32-mm nominal length with applied dots inside machine grips.

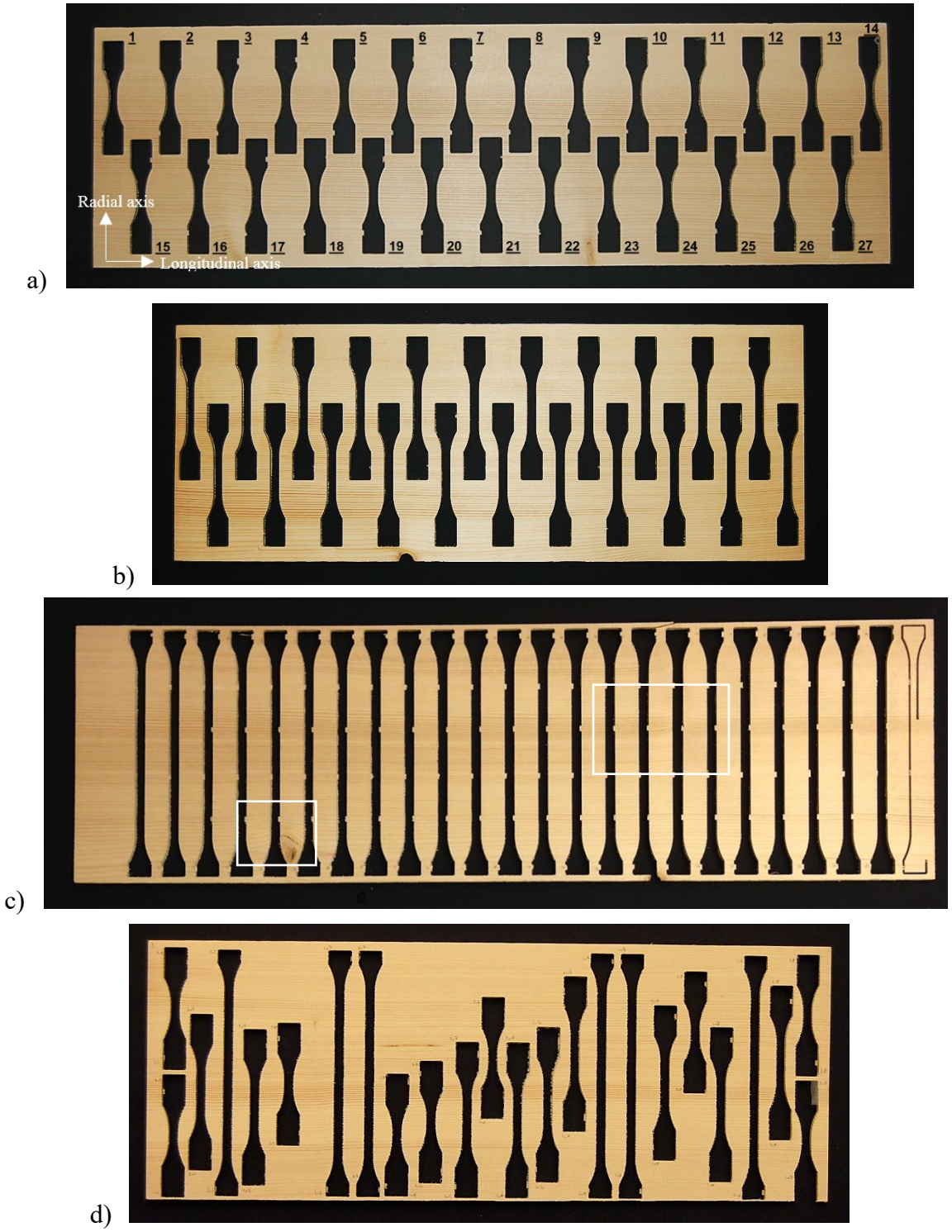


**Fig. 4.** Boards with regular arrangement of specimens: a) 8-mm specimens, b) 32-mm specimens, c) 120-mm specimens (white rectangles show areas affected by knots). d) Random arrangement of specimens of all three lengths.

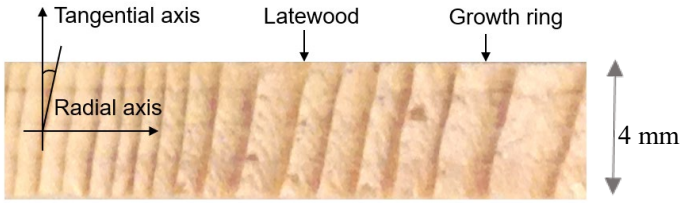


**Fig. 5.** Change of the angle between the local tangential and radial directions, and latewood and growth ring thickness change

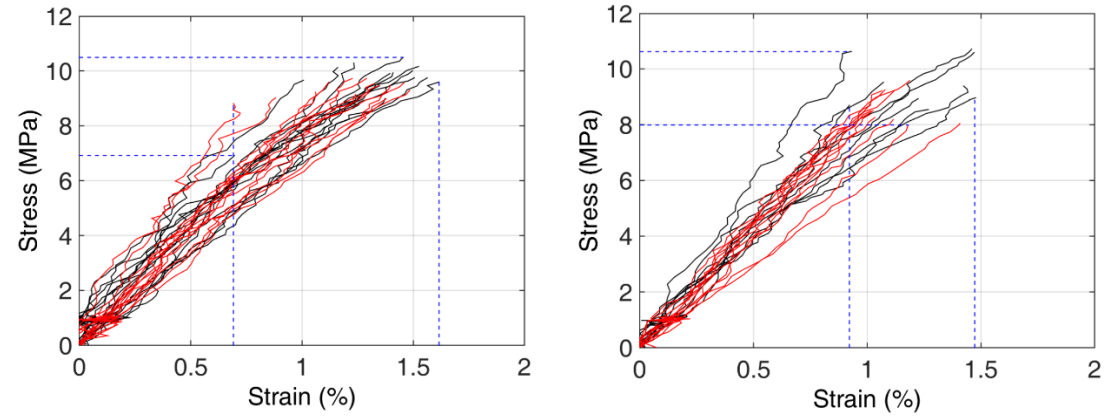


**Fig. 6.** Transverse tensile stress-strain curves of spruce wood for 8-mm specimens cut from REB1 (left) and REB2 (right).

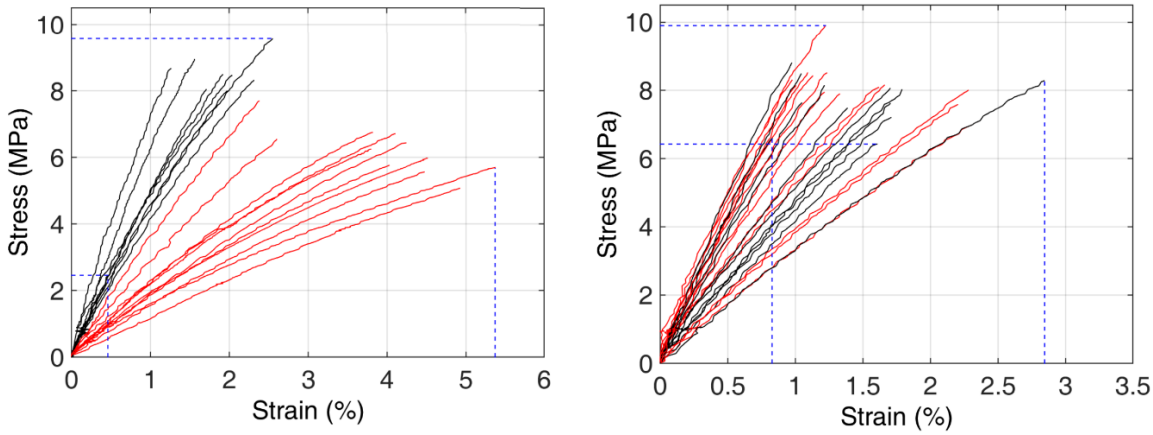


**Fig. 7.** Transverse tensile stress-strain curves of spruce wood for 32-mm specimens cut from REB3 (left) and REB4 (right).

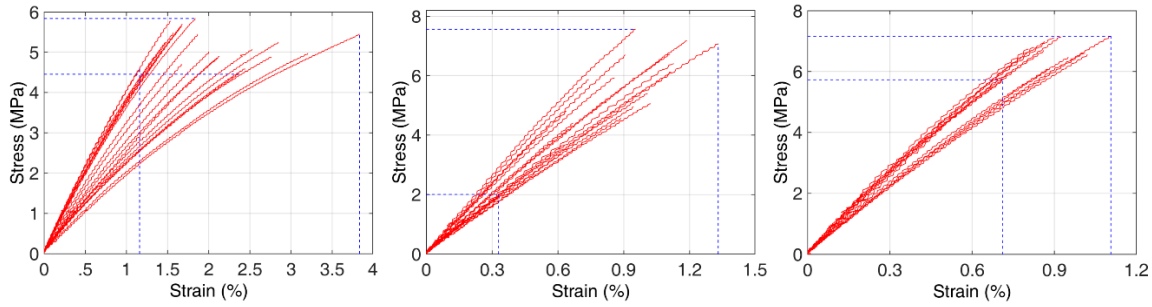


**Fig. 8.** Transverse tensile stress-strain curves of spruce wood for 120-mm specimens cut from REB5-REB7 (left-right).

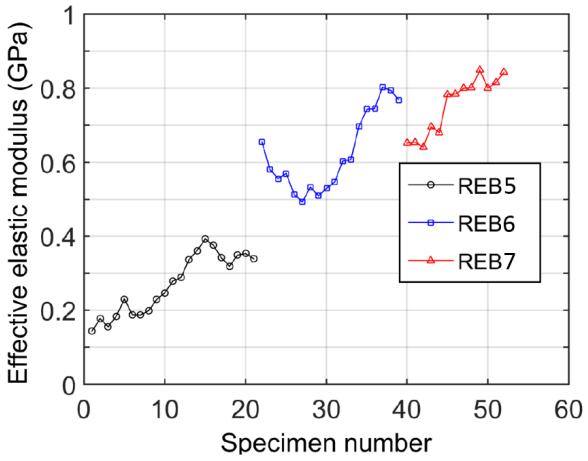


**Fig. 9.** Distribution of effective elastic modulus in the REBs for 120 mm specimens.

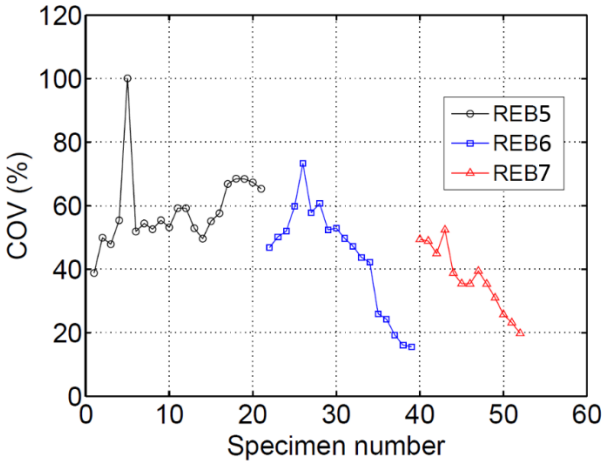


**Fig. 10.** Coefficient of variation for local elastic modulus of each 120-mm specimen in the REBs.

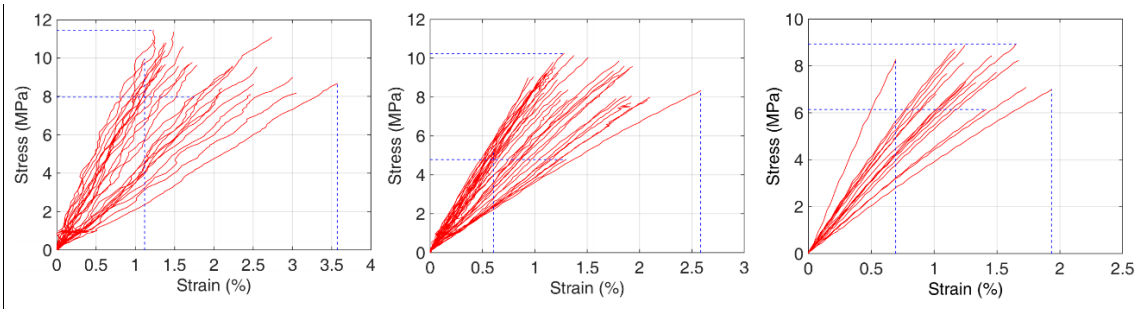


**Fig. 11.** Transverse tensile stress-strain curves of spruce wood for 8-mm specimens (left), 32-mm specimens (middle) and 120-mm specimens (right), cut from RABs.

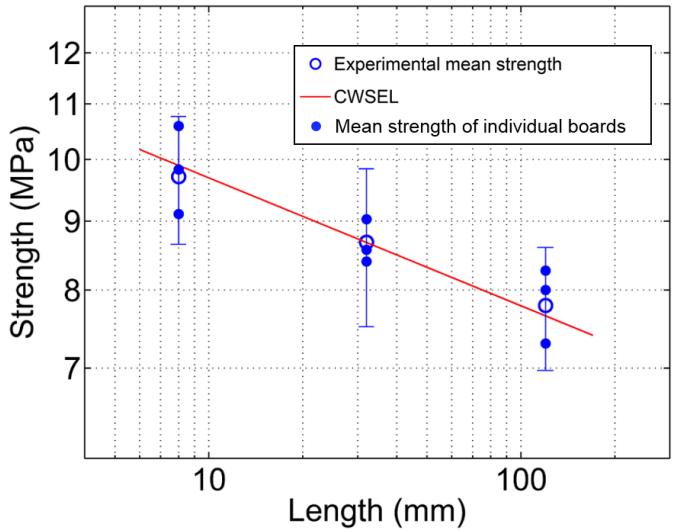


**Fig. 12.** Mean strengths and variations for RAB specimens vs. lengths.

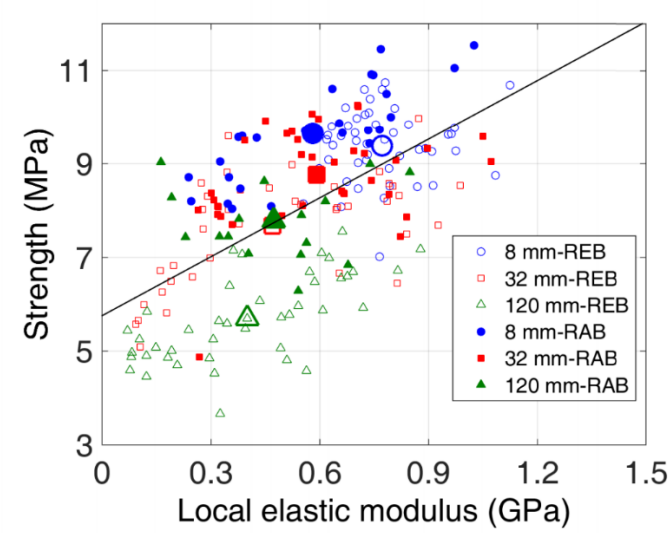


**Fig. 13.** Correlation between local elastic modulus and tensile transverse strength.

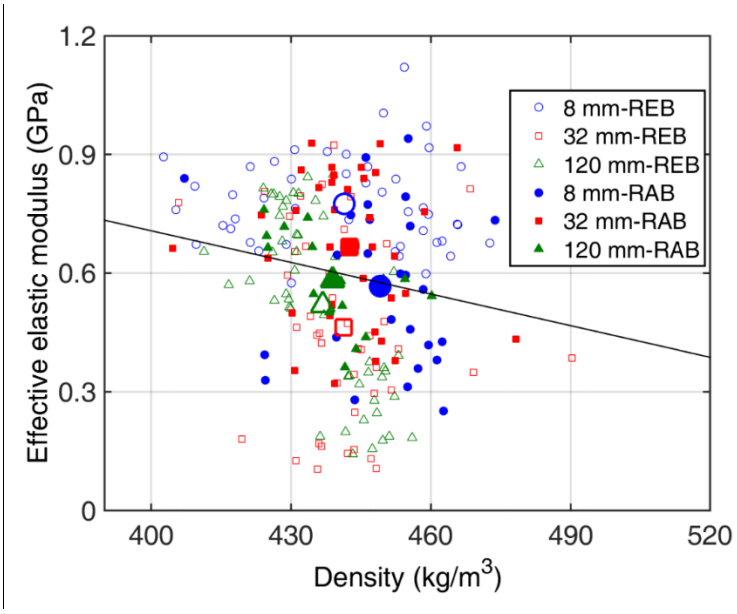


**Fig. 14.** Correlation between density and effective elastic modulus.

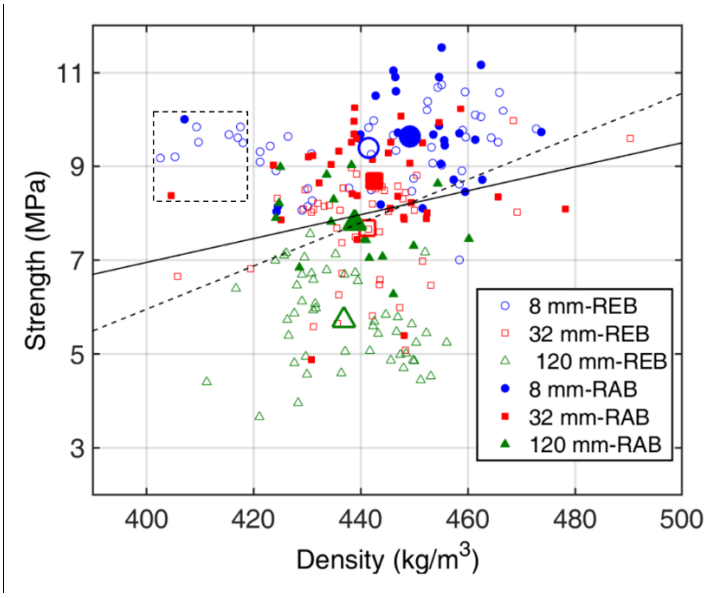


**Fig. 15.** Correlation between density and tensile transverse strength. Solid line – regression line for all data, dashed line – regression excluding the outliers (data in the box)

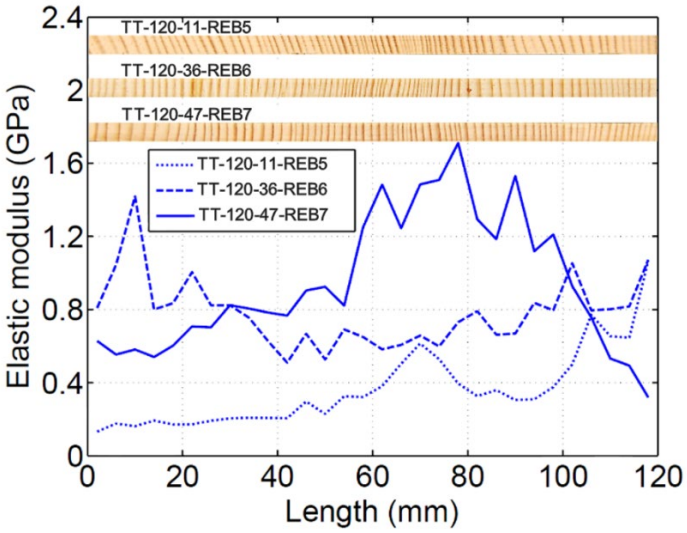


**Fig. 16.** Correspondence between mesostructure of spruce and local transverse elastic modulus.


**Fig. 17.** Different failure modes observed in specimens: a) Earlywood failure, b) Earlywood-border failure, c) Growth ring border failure, d) Crossing growth ring failure. Vertical dimension is 4mm (specimen width). Load is applied along the radial axis.

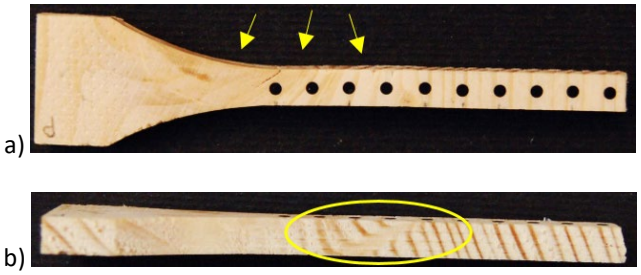


**Fig. 18.** Part of the specimen TT-120-05-REB5 after failure. a) Top view, b) Side view.

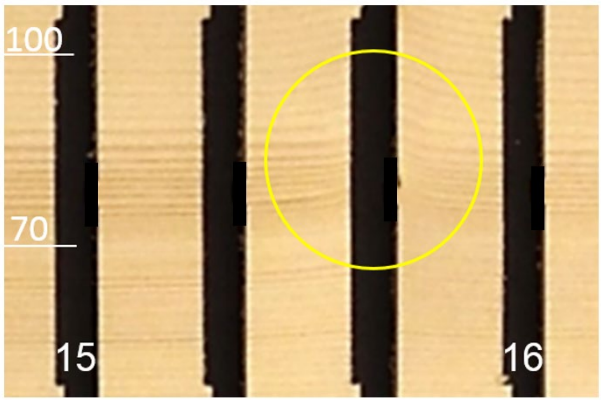


**Fig. 19.** Area affected by a small knot in REB5 (two cut specimens between specimens 15 and 16 were unusable and excluded).


**Fig. 20.** Mesostructure of specimens TT-120-14-REB5 (top), TT-120-15-REB5 (middle) and TT-120-16-REB5 (bottom). Dimensions are in mm.

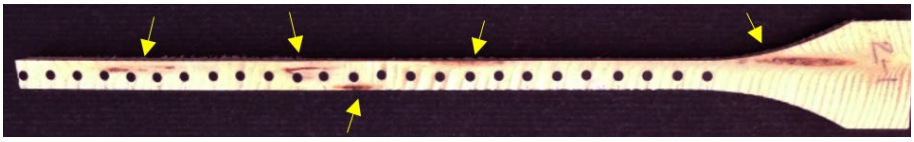

**Fig. 21.** Specimen TT-120-59-RAB2 with knots.


**Fig. 22.** Specimen TT-032-02-REB3 with a resin check.